RNA-binding protein hnRNPLL regulates mRNA splicing and stability during B-cell to plasma-cell differentiation

Xing Chang[a,b], Bin Li[c], and Anjana Rao[a,b,d,e,1]

Divisions of [a]Signaling and Gene Expression and [c]Vaccine Discovery, La Jolla Institute for Allergy and Immunology, La Jolla, CA 92037; [b]Sanford Consortium for Regenerative Medicine, La Jolla, CA 92037; and [d]Department of Pharmacology and [e]Moores Cancer Center, University of California at San Diego, La Jolla, CA 92093

Contributed by Anjana Rao, December 2, 2014 (sent for review July 20, 2014)

Posttranscriptional regulation is a major mechanism to rewire transcriptomes during differentiation. Heterogeneous nuclear RNA-binding protein LL (hnRNPLL) is specifically induced in terminally differentiated lymphocytes, including effector T cells and plasma cells. To study the molecular functions of hnRNPLL at a genome-wide level, we identified hnRNPLL RNA targets and binding sites in plasma cells through integrated Photoactivatable-Ribonucleoside-Enhanced Cross-Linking and Immunoprecipitation (PAR-CLIP) and RNA sequencing. hnRNPLL preferentially recognizes CA dinucleotide-containing sequences in introns and 3′ untranslated regions (UTRs), promotes exon inclusion or exclusion in a context-dependent manner, and stabilizes mRNA when associated with 3′ UTRs. During differentiation of primary B cells to plasma cells, hnRNPLL mediates a genome-wide switch of RNA processing, resulting in loss of B-cell lymphoma 6 (Bcl6) expression and increased Ig production—both hallmarks of plasma-cell maturation. Our data identify previously unknown functions of hnRNPLL in B-cell to plasma-cell differentiation and demonstrate that the RNA-binding protein hnRNPLL has a critical role in tuning transcriptomes of terminally differentiating B lymphocytes.

RNA binding proteins | plasma cells | alternative splicing | PAR-CLIP | hnRNP

In response to pathogen challenge, lymphocytes undergo activation and differentiation into effector cells to exert their physiological functions. This process is accompanied by dramatic changes in cellular transcriptomes and proteomes. Although many of these changes occur through alterations in gene transcription, posttranscriptional regulation of mRNA expression is also a major mechanism for rewiring the transcriptome and increasing proteome diversity during cell differentiation (1). Posttranscriptional regulation is mediated through diverse mechanisms of mRNA processing, including alternative splicing of pre-mRNA, 3′ UTR regulation, and translational control—all typically mediated through interactions between RNA-binding proteins (RBPs) and their target sequences on RNA (2). The accurate mapping of RBP-binding sites on mRNA is critical for elucidating the functions of RBPs and the mechanisms by which they regulate pre-mRNA processing.

The emergence of genome-wide approaches has greatly facilitated our ability to map RBP-binding sites on RNA and explore the mechanisms regulating mRNA alternative processing. RNA–protein interactions have been explored through RNA cross-linking and immunoprecipitation (RNA-CLIP), a method that uses UV irradiation to cross-link RNA to its binding proteins, followed by immunoprecipitation of selected RBPs and next-generation sequencing to identify RNAs bound to those RBPs at a genome-/transcriptome-wide level (3–7). A recent improvement known as PAR-CLIP (Photoactivatable-Ribonucleoside-Enhanced Cross-Linking and Immunoprecipitation) uses a photoactive ribonucleotide analog to increase the efficiency of RNA/protein cross-linking (8). A further advantage of PAR-CLIP is that the polymerases used to reverse-transcribe the cross-linked RNAs tend to introduce specific T-to-C mutations within or in the near vicinity of the RBP-binding sites, thus validating the specificity of RBP binding to coprecipitating RNAs and mapping RBP-binding sites on the validated RNAs at close to single-nucleotide resolution (8).

Heterogeneous nuclear RNA-binding proteins (hnRNPs) is the term applied to a collection of unrelated nuclear RBPs. hnRNPLL was identified through a targeted lentiviral shRNA screen for regulators of CD45RA to CD45RO switching during memory T-cell development (9) and independently through two separate screens performed by different groups for exclusion of CD45 exon 4 in a minigene context (10) and for altered CD44 and CD45R expression on T cells in *N*-ethyl-*N*-nitrosourea (ENU)-mutagenized mice (11). Mice with an ENU-induced mutant allele of *Hnrpll* (which encodes hnRNPLL) showed defects in T-cell survival and homeostasis (11). hnRNPLL is up-regulated during T-cell activation; it also is highly expressed in plasma cells, where it regulates the switching between membrane and secreted Ig in a plasma cell line (12). However, the role of hnRNPLL during primary plasma cell differentiation is not known. Moreover, although exon arrays comparing wild-type and hnRNPLL-deficient T cells have provided a global view of hnRNPLL-mediated alternative splicing events in T cells (9, 11), such approaches are typically unable to discriminate direct and indirect effects, because splicing factors are well known to regulate the processing of mRNAs encoding other splicing factors (13, 14). Whether hnRNPLL is involved in RNA processing beyond inducing exon exclusion also remains to be determined. In this study, therefore, we generated a transcriptome-wide map of the direct sites of interaction of hnRNPLL with RNA, so as to increase our understanding of the roles of hnRNPLL in RNA alternative processing during lymphocyte differentiation.

Significance

Plasma cells produce immunoglobulin and provide long-lasting protective immunity. Differentiation of B cells to plasma cells is accompanied by major changes in gene expression, which are regulated at both transcriptional and posttranscriptional levels. We have used genome-wide methods to identify the binding sites and RNA targets of heterogeneous nuclear RNA-binding protein LL (hnRNPLL), whose expression is up-regulated during B-cell to plasma-cell differentiation. In addition to its recognized function in promoting exon splicing, hnRNPLL shapes the transcriptome of plasma cells by regulating exon inclusion and promoting mRNA stability. hnRNPLL binds to preferred sequences in RNA and is critical for complete plasma-cell differentiation, by mediating the down-regulation of B-cell–specific transcription factors and maximizing immunoglobulin production.

Author contributions: X.C. and A.R. designed research; X.C. performed research; X.C., B.L., and A.R. analyzed data; and X.C. and A.R. wrote the paper.

The authors declare no conflict of interest.

Data deposition: The sequence reported in this paper has been deposited in the Sequence Read Archive (SRA) database (accession no. SRP056204).

[1]To whom correspondence should be addressed. Email: arao@liai.org.

This article contains supporting information online at www.pnas.org/lookup/suppl/doi:10.1073/pnas.1422490112/-/DCSupplemental.

Plasma cells are terminally differentiated B lymphocytes that lose their B-cell characteristics and acquire the capacity to produce large quantities of antibodies. Plasma cells are the major source of antibodies for humoral immunity. The differentiation of plasma cells from B cells requires an extensive reorganization of transcriptional programs, a process mainly mediated by two antagonistic transcription factors, B-cell lymphoma 6 (Bcl6) and B-lymphocyte–induced maturation protein 1 (Blimp1) (15). During plasma-cell differentiation, the differentiating B cells acquire plasma-cell–specific transcription factors, such as Blimp1 and X-box–binding protein 1 (Xbp1), and terminate the expression of B-cell–specific transcription factors, including Bcl6 and Pax5 (16). Plasma-cell differentiation is also accompanied by alteration of mRNA alternative processing: The mRNA encoding the transmembrane phosphatase CD45 undergoes alternative splicing to exclude exons 4–6, thus switching the CD45 protein from its highest-molecular-weight isoform, CD45RABC (also known as B220 in B cells), to the lowest-molecular-weight isoform, CD45RO (17, 18). However, the role of posttranscriptional regulation in plasma-cell differentiation is less well characterized than the analogous process in T cells (1, 6, 9–11, 19).

In the B-cell lineage, hnRNPLL is minimally expressed at the naïve B-cell stage, but is up-regulated significantly after B-cell differentiation into plasma cells (12). In this study, we have carried out PAR-CLIP analysis of hnRNPLL in plasma cells and combined it with deep RNA sequencing (RNA-seq) to identify hnRNPLL-dependent regulatory events in plasma cells. We show that in plasma cells, hnRNPLL preferentially associates with CA-repeat RNA sequences in introns and 3′ UTRs and can either enhance or suppress the inclusion of alternative exons depending on its location relative to exon–intron junctions. Unexpectedly, we also found that the association of hnRNPLL with 3′ UTRs increases RNA stability. In the absence of hnRNPLL, the termination of Bcl6 expression and optimal Ig production in plasma cells were both compromised, indicating that RNA alternative processing mediated by hnRNPLL has an important role in plasma-cell development and function.

Results

PAR-CLIP Identifies hnRNPLL-Binding Sites on RNA of Plasmacytoma Cells. To systemically identify hnRNPLL-binding sites on RNA in vivo, we used the recently established PAR-CLIP technique (8) (outlined in Fig. S1). Briefly, we pulsed a plasmacytoma cell line, MPC11, with the photoreactive ribonucleoside analog 4-thiouracil (4-SU; Fig. S1*A*) for 12–14 h. The cells were then irradiated with UV light (365 nm) to induce covalent RNA–protein cross-linking, after which hnRNPLL and its cross-linked RNAs were immunoprecipitated with our previously generated anti-hnRNPLL antibody (12). The proteins in the immunoprecipitate were resolved by SDS polyacrylamide gel electrophoresis (SDS/PAGE), and the hnRNPLL/RNA complex was excised from the gel after visualization with an RNA dye, SYBR green II (Fig. 1*A*). The antibody pulled down the canonical isoform of hnRNPLL as well as another isoform of higher molecular weight (Fig. 1*A*), generated through the use of a noncanonical translational start site (CUG) located 5′ of the canonical ATG start codon (Fig. S2*A*). The longer hnRNPLL isoform was also expressed in primary plasma cells (Fig. S2*C*). Both isoforms were associated with RNA based on SYBR green staining; we focused on the more abundant canonical isoform for the following analyses. After the cross-linked RNAs were recovered from the hnRNPLL/RNA complex, they were ligated to RNA adaptors, converted into cDNA, and sequenced on the SOLiD high-throughput sequencing platform (Fig. S1*B*).

With this approach, in two independent experiments, we obtained >50 × 10^6 high-quality reads corresponding to hnRNPLL-binding RNAs, from which we derived ∼110,000 hnRNPLL-binding sites and ∼6,000 genes whose transcripts were bound by hnRNPLL (Table S1). More than 40% of the reads contained the T-to-C mutations characteristic of PAR-CLIP that are introduced through misincorporation by reverse transcriptase (8) (Fig. 1*B*), indicating high cross-linking efficiency in our assays. The most enriched Gene Ontology terms for transcripts bound by hnRNPLL were related to RNA processing (Fig. 1*D*), consistent with previous findings that hnRNP proteins largely regulate alternative processing of pre-mRNAs encoding splicing factors (13, 14). The hnRNPLL PAR-CLIP results were reproducible, with a large overlap between the hnRNPLL-binding transcripts identified in two independent experiments (Fig. 1*C*). Therefore, using the PAR-CLIP approach, we have successfully mapped the interaction sites of hnRNPLL on the RNAs to which it binds in plasmacytoma cells.

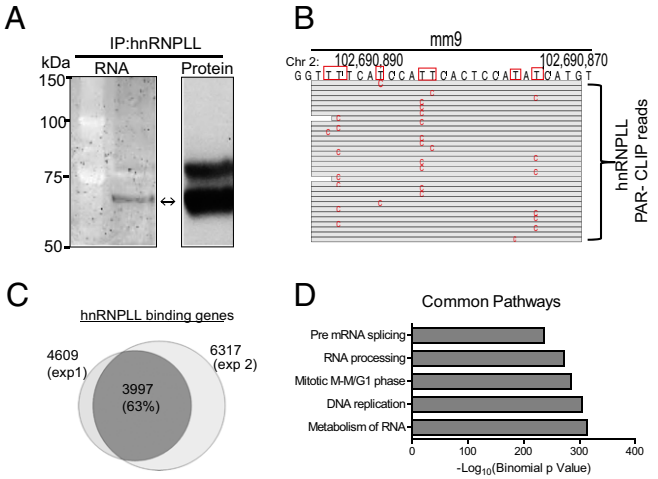

Fig. 1. PAR-CLIP identifies hnRNPLL-associated RNAs in MPC11 cells. (*A*) Isolation of hnRNPLL/RNA complex by immunoprecipitation. (*A*) hnRNPLL was immunoprecipitated from MPC11 cells, and the immunoprecipitated proteins were resolved on SDS/PAGE and stained with SYBR-Green II to visualize cross-linked RNA (*Left*) or immunoblotted with the anti-hnRNPLL antibody (*Right*). The double arrow indicates the band corresponding to the canonical isoform of hnRNPLL based on its predicted molecular weight. (*B*) A representative hnRNPLL-binding site on *Cd44* mRNA. The sequence of a binding region on *Cd44* mRNA is depicted at the top. Sequences from hnRNPLL PAR-CLIP reads were aligned to the mRNA sequence, and sites of T > C conversion observed in individual reads are indicated. (*C*) PAR-CLIP consistently identifies hnRNPLL-binding mRNA targets. Two independent PAR-CLIP experiments were conducted, and genes containing hnRNPLL-binding sites were identified. The overlap of the two gene lists is depicted in the Venn diagram. (*D*) hnRNPLL-associated transcripts are enriched for RNA-processing events. hnRNPLL-associated transcripts were analyzed for Gene Ontology by using DAVID (42). The top five enriched terms of common pathways are listed.

hnRNPLL Preferentially Binds (CA)n Motifs in Introns and 3′ UTRs of Pre-mRNA Transcripts. We examined the distribution of hnRNPLL-binding sites on mRNA transcripts. Based on Ref-seq annotations, >80% of hnRNPLL binding sites fell into the transcribed regions of annotated genes; ∼70% of these binding sites were located within introns, confirming that our PAR-CLIP experiments captured pre-mRNA (Fig. 2*A*). Predominant intronic binding is also consistent with the nuclear location of hnRNPLL and its established function as a regulator of pre-mRNA splicing. Unexpectedly, however, 10% of the hnRNPLL-binding sites fell into 3′ UTR regions (Fig. 2*A*)—much higher than the proportion of 3′ UTRs in the genome (3%), suggesting an unappreciated function for hnRNPLL in regulating 3′ UTR activity.

To identify RNA sequences that were recognized by hnRNPLL, we used the MEME-ChIP de novo motif identification algorithm (20). (CA)n emerged as the most highly enriched sequence in both intronic and 3′ UTR binding sites of hnRNPLL (Fig. 2 *B* and *C*), indicating that hnRNPLL preferentially recognizes CA dinucleotide repeats on RNA. Interestingly, a systematic evolution

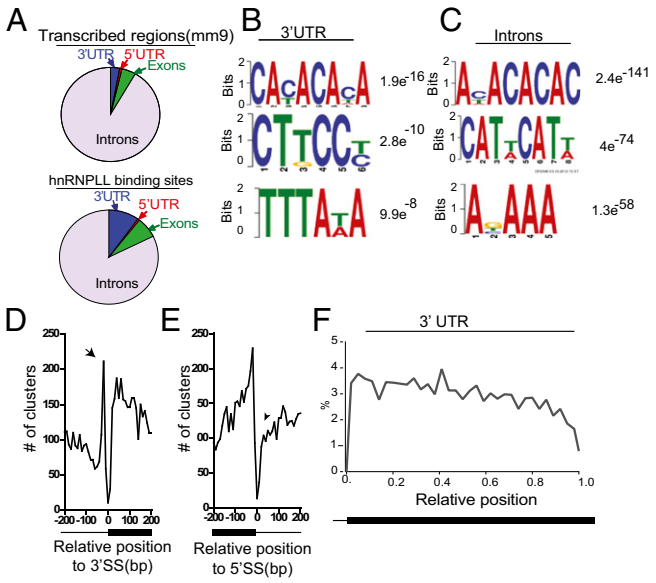

Fig. 2. hnRNPLL recognizes tandem (CA) diribonucleotide repeats and other motifs in RNA. (*A*) Distribution of hnRNPLL-binding clusters among coding exons, introns, and 5′ and 3′ UTRs (*Lower*); the genomic ratios of the same elements are shown as a control (*Upper*). Note that the percentage of hnRNPLL-binding sites in 3′ UTR (10%) is much more than the genomic ratios of 3′ UTR (3%). (*B* and *C*) hnRNPLL recognizes (CA)n RNA motifs. Sequences of hnRNPLL-binding sites on either 3′ UTRs (*B*) or introns (*C*) were extracted and used as input for MEME-Chip motif identifier (20) to derive the most enriched sequences. The top three enriched motifs and their *P* values are depicted. (*D* and *E*) hnRNPLL-binding sites are enriched at 3′ splice sites (3′-SS), but not 5′ splice sites (5′-SS). The distance between the center of hnRNPLL-binding sites and 3′-SS (*D*) or 5′-SS (*E*) was calculated, and the distribution was plotted. The arrow in *D* depicts the enrichment of hnRNPLL clusters 5′ of the 3′-SS; the arrowhead in *E* shows lack of enrichment at the 5′ splice sites. (*F*) hnRNPLL-binding clusters were enriched at the proximal end of 3′ UTRs. As in *D*, the distance of hnRNPLL-binding sites relative to the start of 3′ UTRs was plotted. A.U., arbitrary units.

of ligands by exponential enrichment (SELEX) experiment conducted on hnRNP L, a close relative of hnRNPLL, also revealed a preference for (CA) repeats (21), suggesting that these two closely related splicing factors may share similar binding motifs on RNAs.

We further examined the location of hnRNPLL-binding sites with respect to intron–exon boundaries in pre-mRNA. We observed an increased frequency of binding in the intron immediately upstream of 3′ splice sites, but no increase in the frequency of binding downstream of 5′ splice sites (Fig. 2 *D* and *E*), suggesting that hnRNPLL acts predominantly through 3′ splice sites. Intron/exon junctions, which are often G-rich, essentially lacked hnRNPLL-binding clusters, most likely reflecting RNase T1-mediated cleavage downstream of guanine nucleotides during the PAR-CLIP protocol (22). Moreover, hnRNPLL-binding sites were slightly enriched toward the proximal ends of 3′ UTR exons (Fig. 2*F*).

hnRNPLL Regulates RNA Splicing in a Context-Dependent Manner. To investigate how hnRNPLL regulates RNA processing, we depleted hnRNPLL protein (Fig. 3*A* and Fig. S2*B*) and Hnrpll transcript (Fig. 4*B*) in MPC11 cells using two independent shRNAs, and then performed RNA-seq analysis in these LL-deficient cells (ShLL1 and ShLL2), as well as in control MPC11 cells expressing control shRNA against GFP (ShGFP). We obtained ∼80 million paired-end reads from two biological replicates and analyzed our RNA-seq data using the MISO (Mixture of Isoforms) program to identify alternative pre-mRNA splicing events mediated by hnRNPLL (23). The ψ (PSI; percentage of spliced in) score, defined as the percentage of transcripts containing the alternative exon, was used to compare splicing efficiencies in ShLL and ShCtrl cells for all annotated alternative splicing events in the mouse transcriptome (Fig. 3*B*); the highest proportion of hnRNPLL-mediated events involved changes in alternative first or last exon use or skipped exons, with tandem UTR choices also relatively frequent (Fig. 3*B*). Gene Ontology analysis of these hnRNPLL-mediated RNA alternative processing events suggests involvement of hnRNPLL in key plasma-cell functions, including protein translation, intracellular transport, and protein localization (Fig. S3*A*).

Focusing on exclusion or inclusion of cassette exons, the best-characterized splicing events, we found that splicing patterns of 250 cassette exons were altered after hnRNPLL depletion, with 150 cassette exons showing increased inclusion ($\Delta\ \psi > 0.2$) and the remaining 100 cassette exons showing decreased inclusion ($\Delta\ \psi < -0.2$) under the same conditions. Representative data (see below and Fig. 3 *C*, *D*, *F*, and *G*) were confirmed by RT-PCR (Fig. 3 *E* and *H* and Fig. S3 *B* and *C*). Therefore, in addition to its canonical role of promoting exon exclusion, hnRNPLL also enhances exon inclusion in MPC11 cells.

To further determine whether the location of hnRNPLL binding relative to an exon influenced exon inclusion/exclusion, we considered the combined data from RNA-seq and PAR-CLIP analyses. Considering only hnRNPLL-binding sites either 1 kb upstream or downstream of exons, we found that 29 of 100 (29%) exons with decreased inclusion ($\Delta\psi < -0.2$) had hnRNPLL-binding sites within this window, compared with 54 of 150 (36%) exons showing increased inclusion ($\Delta\psi > 0.2$). For exons whose inclusion was increased after hnRNPLL depletion ($\Delta\psi > 0.2$), hnRNPLL-binding sites tended to occur 3′ of the exon: For example, hnRNPLL bound to a region 3′ of exon 2b of *Phf15* pre-mRNA (Fig. 3*C*), and its depletion was associated with increased inclusion of this exon (ψ score changed from 0.24 to 0.91, Fig. 3*D*; RT-PCR confirmation, Fig. 3*E*). In contrast, for exons whose inclusion was decreased after hnRNPLL depletion ($\Delta\psi < -0.2$), hnRNPLL-binding sites tended to occur 5′ of the exon; for instance, hnRNPLL bound to a region 5′ of an alternative exon in *Ube3a* (Fig. 3*F*), and its depletion was associated with reduced inclusion of this exon (ψ score changed from 0.73 to 0.09; Fig. 3 *G* and *H*). Analysis of all 250 exons provided a global confirmation of this observation (Fig. 3 *I* and *J*). Therefore, we propose that hnRNPLL regulates splicing of cassette exons in a context-dependent manner: hnRNPLL binding 5′ of cassette exons tends to promote their inclusion, whereas hnRNPLL binding at 3′ of cassette exons tends to promote their exclusion.

We note that a relatively small percentage of hnRNPLL-regulated cassette exons contain hnRNPLL-binding sites nearby (within 1 kb either downstream or upstream), and in fact there is no significant difference in the number of hnRNPLL-binding sites upstream and downstream of these exons (Mann–Whitney test: $P = 0.563$ for Fig. 3*I*; $P = 0.355$ for Fig. 3*J*). However, this lack of significance does not necessarily mean that the remaining exons are indirectly affected by hnRNPLL, because many of them have hnRNPLL-binding sites at distal regions of introns (>1 kb away from exons). The significance of hnRNPLL binding at distal intronic regions remains to be determined.

hnRNPLL Binding at the 3′ UTR Increases mRNA Stability in Cells. Besides their enrichment in coding exons and introns, hnRNPLL-binding sites were also significantly enriched within 3′ UTRs in our PAR-CLIP analysis (Fig. 2*A*). Because the 3′ UTR is the most important *cis*-element that regulates RNA stability, we analyzed the expression of genes whose transcripts contained hnRNPLL-binding sites in their 3′ UTRs. Transcripts containing hnRNPLL-binding sites within their 3′ UTR regions showed significantly lower expression when hnRNPLL was depleted compared with transcripts lacking hnRNPLL binding. For instance, two of the most strongly down-regulated genes in hnRNPLL-depleted cells, *Crip2* and *Slx1b*, both had strong and specific hnRNPLL

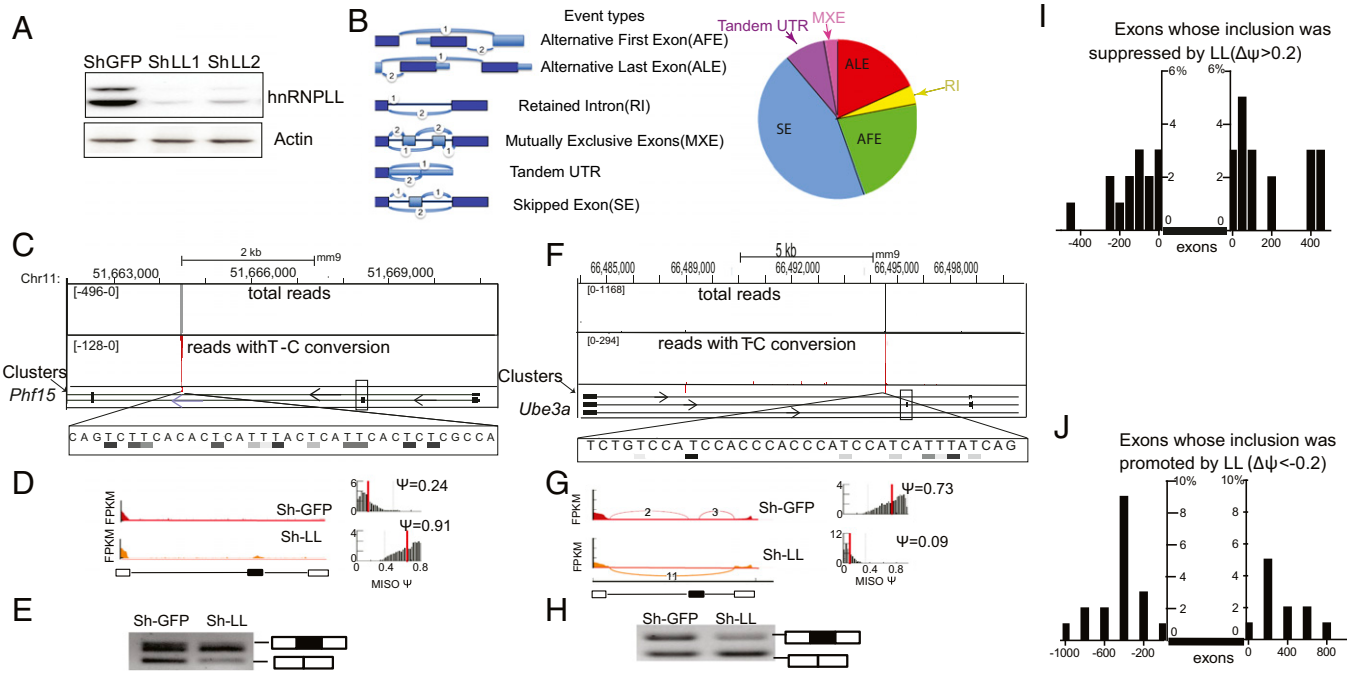

Fig. 3. hnRNPLL regulates RNA alternative splicing in a context-dependent manner. (*A*) Two different shRNAs against *Hnrpll* efficiently eliminated the expression of both hnRNPLL isoforms in MPC11 cells. MPC11 cells were stably transduced with pLKO.1 sh-*Hnrpll* shRNAs (sh-LL1 or sh-LL2) or pLKO.1 sh-GFP shRNA (sh-Ctrl), and hnRNPLL protein expression was determined by immunoblot analysis. The target regions of the two shRNAs are depicted in Fig. S2*B*. (*B*, *Left*) Schemes depict different types of alternative splicing events. Number 1 and 2 represent two different splicing outcomes. (*B*, *Right*) RNA-seq analysis identifies categories of alternative RNA-processing events mediated globally by hnRNPLL. RNA-seq results were analyzed with the MISO algorithm (23) to determine significantly changed alternative splicing events in MPC11 cells after hnRNPLL depletion. Pie chart depicts types of alternative splicing events that were significantly changed after hnRNPLL depletion ($\Delta\psi < -0.2$ or $\Delta\psi > 0.2$). (*C*–*E*) hnRNPLL binds 3′ of exon 2b of the *Phf15* gene and promotes its exclusion. (*C*) Genome browser view of PAR-CLIP results on *Phf15* transcripts. Tracks from top to bottom represent the following: the number of PAR-CLIP reads (scale is shown in square brackets at top left, and minus number represents mapping on the reverse strand); the number of reads containing T > C transitions, indicative of sites of protein–RNA cross-linking; identified clusters of PAR-CLIP reads, which indicate hnRNPLL-binding sites; and the Ref-seq annotation of the *Phf15* gene. The nucleotide sequence of the cluster is shown below, with the T's indicated on a gray scale that depicts the frequency of T > C conversion at that T. Note: The *Phf15* gene was transcribed from the minus strand of DNA, and so were the mapped PAR-CLIP reads. (*D*) hnRNPLL promotes exclusion of exon 2b (boxed) in the *Phf15* gene. RNA-seq experiments were performed by using MPC-11 cells with stable transfection of sh-RNA against hnRNPLL (sh-LL-1) or against GFP (sh-Ctrl). RNA-seq results were mapped by using Tophat, and the percentage of inclusion (Ψ) of the cassette exons was calculated with the MISO program (22). (*E*) RT-PCR analysis validates that hnRNPLL depletion results in increased inclusion of *Phf15* exon 2b. cDNA was prepared from MPC-11 cells stably transduced with shRNA as described above. PCR primers were designed to localize at the flanking constant exons. The upper band of the PCR products is derived from the isoform that includes exon 2b, whereas the lower band represents the isoform that excludes this exon. The data are representative of two independent experiments. (*F*–*H*) hnRNPLL binding 5′ of a cassette exon in the *Ube3a* gene promotes exon inclusion. (*F*) As in *C*, depicts hnRNPLL-binding sites 5′ of a cassette exon (boxed) in the *Ube3a* gene. (*G*) Analysis of alternative splicing of the indicated cassette exon in the *Ube3a* gene with MISO. (*H*) RT-PCR confirms that hnRNPLL depletion results in increased exclusion of the indicated cassette exon. (*I*) hnRNPLL binding 3′ of a cassette exon tends to suppress its inclusion. hnRNPLL-binding sites at exons whose inclusion was increased after hnRNPLL depletion ($\Delta\Psi > 0.2$) were analyzed for the distribution of hnRNPLL-binding clusters. hnRNPLL binding occurs more frequently within a 1-kb region 3′ of these exons than within the corresponding 1-kb region 5′ of the exons, suggesting that hnRNPLL binding 3′ of a cassette exon promotes its exclusion. (*J*) As in *I*, cassette exons whose inclusion was decreased after hnRNPLL knockdown ($\Delta\Psi < -0.2$) were analyzed for hnRNPLL-binding sites. There is more hnRNPLL binding 5′ of these exons, suggesting that hnRNPLL binding 5′ of a cassette exon promotes its inclusion. RNA-seq and MISO analyses of alternative splicing are representative of two experiments.

binding in their 3′ UTRs (Fig. 4 *A* and *B*). Analysis at the genome-wide level further supported such conclusions: For transcripts lacking hnRNPLL binding, the number of transcripts whose expression was significantly suppressed after hnRNPLL knockdown was similar to the number of transcripts whose expression was increased. In contrast, for transcripts that displayed hnRNPLL binding at their 3′ UTRs, more transcripts were suppressed than increased (Fig. 4*C*). Similarly, genes with hnRNPLL binding at their 3′ UTRs had significantly decreased expression after hnRNPLL depletion, in contrast to the genes lacking hnRNPLL binding (Fig. 4*D*). Based on this analysis, we concluded that hnRNPLL binding at 3′ UTRs enhances mRNA stability in cells. Supporting its function in regulating 3′ UTR activity, we found that hnRNPLL was present both in the cytoplasm and in the nucleus (Fig. S3*D*).

Together, our results from our integrated genome-wide RNA-seq and PAR-CLIP analyses reveal a previously unidentified function of hnRNPLL in regulating mRNA stability, as well as a context-dependent role for hnRNPLL in pre-mRNA alternative splicing.

hnRNPLL Indirectly Suppresses Bcl6 Expression and Regulates Ig Production in Plasma Cells. Naïve B cells rapidly divide and differentiate into plasma cells in vitro after Toll-like receptor stimulation (24). We therefore used an in vitro LPS-induced plasma-cell differentiation assay to analyze hnRNPLL expression during plasma-cell differentiation. As expected, hnRNPLL was minimally expressed in naïve B cells, but was drastically up-regulated after three to four cycles of cell division after activation of B cells with LPS or anti-CD40 in the presence of the cytokines IL-4 and IL-5 (Fig. 5*A* and Fig. S4*A*, *Upper*). At day 5 after activation, hnRNPLL was most highly expressed in cells with plasma-cell phenotypes—i.e., cells expressing the plasma-cell marker CD138 and the transcription factor Blimp1—and cells with lower B220 (CD45RABC) expression. In contrast, activation of B cells with

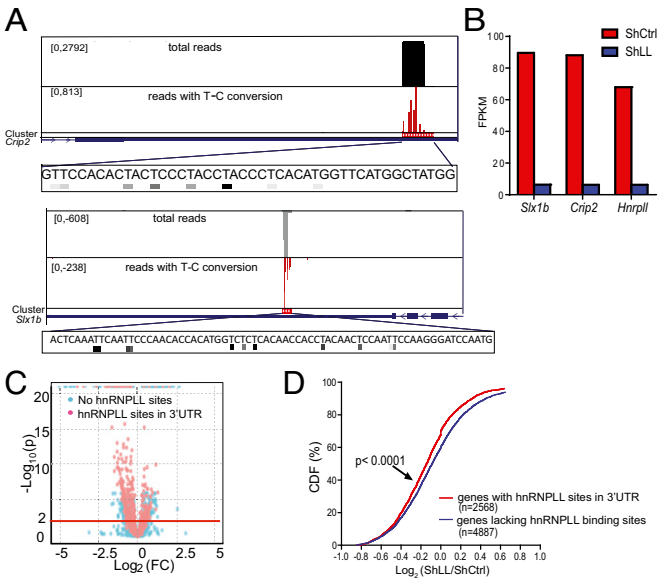

Fig. 4. hnRNPLL binding at 3′ UTRs stabilizes mRNA. (*A*) Genome browser tracks depict binding sites of hnRNPLL on the 3′ UTR of *Crip2* (*Upper*) and *Slx1b* (*Lower*) mRNA. From top to bottom are total mapped PAR-CLIP reads (scale shown in square brackets at top left), reads with T > C conversion, and Ref-seq annotation of the depicted region. The nucleotide sequence of the identified clusters is shown at the bottom, and the density of T > C conversion rates are indicated. (*B*) *Crip2* and *Slx1b* gene expression were significantly decreased after *Hnrpll* knockdown in the MPC11 cells. Gene expression levels (FKPM) were determined with Cuffdiff from the RNA-seq analysis. (*C*) Volcano plot depicts expression changes of genes with hnRNPLL binding at their 3′ UTRs. Log10(p) < −2 was used as cutoff for significantly altered genes (n = 1,547, of which 580 contained hnRNPLL-binding sites at their 3′ UTRs). (*D*) hnRNPLL binding at the 3′ UTR enhances mRNA stability. All genes with hnRNPLL binding at their 3′ UTR (blue line; n = 2,568) were compared with those without hnRNPLL binding (red line; n = 4887) for gene expression change after hnRNPLL depletion. CDF, cumulative distribution function. $P < 0.0001$ in Student's t test. Calculation of FKPM was based on the average of two RNA-seq experiments.

anti-IgM was less effective at inducing plasma-cell differentiation as judged by Blimp-1 and CD138 expression, B220 down-regulation, or hnRNPLL expression (Fig. S4*A*, *Lower*).

We further examined the function of hnRNPLL in plasma-cell differentiation in vitro using ShRNA to deplete *Hnrpll*. Briefly, purified naïve B cells were activated with LPS overnight and infected with retrovirus containing scrambled shRNA (ShCtrl) or two shRNA clones against *Hnrpll* (ShLL1 and ShLL2). Five days after infection, transduced cells were identified by GFP expression and analyzed for plasma-cell markers. As shown in Fig. 5*B*, both shRNAs efficiently reduced hnRNPLL expression in CD138$^+$ plasma cells.

B-cell differentiation into plasma cells is accompanied by a switch from the largest (B220, CD45RABC) to the smallest (CD45RO) isoform of CD45 (17). In cells transduced with either of the two shRNAs against *Hnrpll*, expression of B220 remained higher than in control shRNA transduced cells (Fig. 5*C*, *Upper Left*). This change of B220 expression was mainly because the CD45RA isoform remained up-regulated in the hnRNPLL-depleted cells (Fig. 5*C*, *Upper Right*), whereas expression of the CD45RB or CD45RC isoforms was affected at minimal level (Fig. 5*C*, *Lower*). This flow-cytometric analysis was confirmed by RT-PCR, using PCR primers flanking the alternative RA, RB, and RC exons and amplifying all of the splicing isoforms of CD45 (Fig. 5*D* and Fig. S5*A*). In the hnRNPLL-depleted cells, the PCR product corresponding to B220 (CD45RABC) isoform was significantly more abundant than in the control cells, whereas the PCR products of the other spliced isoforms were much less. Thus, hnRNPLL selectively mediates the exclusion of CD45 exon 4, encoding CD45RA, during plasma-cell differentiation.

Plasma-cell differentiation is regulated by an elaborate transcriptional network mediated by two reciprocally regulated transcription factors, *Bcl6* and *Blimp1* (16, 25). *Bcl6* is highly expressed in germinal center (GC) B cells and promotes their proliferation and survival. During plasma-cell differentiation, expression of *Bcl6* has to be terminated to complete differentiation while *Blimp1* expression is induced. hnRNPLL-depleted plasma cells, generated after 6 d of LPS stimulation in vitro, showed significantly higher expression of *Bcl6* mRNA compared with wild-type plasma cells, suggesting that hnRNPLL acts to suppress *Bcl6* expression in plasma cells (Fig. 5*E*). Consistent with elevated *Bcl6* expression, hnRNPLL-depleted plasma cells expressed a higher level of the proliferation marker Ki-67, indicating that hnRNPLL-depleted plasma cells maintained their proliferation potential compared with control shRNA-transduced cells (Fig. S4*B*). However, Xbp1 and Blimp1, two other key transcription factors in plasma cells, showed no change in their mRNA expression in hnRNPLL-depleted cells (Fig. 5*E*); similarly, hnRNPLL depletion did not change the efficiency of initial plasma-cell differentiation as determined by acquisition of the plasma-cell marker CD138 (Fig. 5*F*). Together, these results indicate that hnRNPLL controls certain, but not all, aspects of commitment to the plasma-cell lineage in vitro.

One of the main properties of plasma cells is their ability to produce large amounts of Ig. In the presence of IL-4, plasma cells mainly produce the Ig IgG1 isoform. Although hnRNPLL depletion did not affect CD138 expression, we found that hnRNPLL-depleted cells produced significantly less IgG1 than the control cells, as determined either by intracellular staining (Fig. 5*G*) or by ELISA (Fig. 5*H*). Class-switching to IgG1, however, was comparable between control shRNA-expressing and hnRNPLL-depleted cells, as determined by percentage of IgG1-producing cells (Fig. 5*G*). The reduced production of IgG1 was not caused by diminished transcription, because mRNA for IgG1 was comparable between control and hnRNPLL-depleted cells (Fig. 5*E*).

In summary, we found that hnRNPLL deficiency was dispensable for the initial steps of transition of differentiating B cells into plasma cells, such as up-regulation of CD138. In contrast, hnRNPLL was required at later stages for complete commitment of differentiating B cells to the plasma-cell lineage, including the CD45 isoform switch, the down-regulation of *Bcl6*, exit from the cell cycle, and the capacity to produce a large quantity of immunoglobulins.

hnRNPLL Plays an Important Role in Determining the Plasma-Cell Transcriptome. To identify hnRNPLL-mediated alternative splicing events during B-cell to plasma-cell differentiation, we purified naïve B cells, in vitro-differentiated CD138$^+$ plasma cells stably expressing control (scramble) shRNA (Ctrl) and plasma cells stably expressing two independent hnRNPLL shRNAs (ShLL1 or ShLL2), and performed RNA-seq. Using the MISO algorithm, we identified 422 RNA cassette exons whose splicing patterns were significantly changed between B cells and sh-Ctrl plasma cells ($\Delta\psi > 0.2$ or < -0.2) and then asked to what extent these splicing events were mediated by hnRNPLL. Fig. 6*A* shows a heat map of ψ values of these plasma-cell–specific splicing events in the indicated cell populations (Table S2). The unsupervised hierarchical cluster analysis revealed two clear clusters in which splicing patterns were consistently reversed in hnRNPLL-depleted plasma cells. Within these alternative splicing events, exclusion of CD45 exon 4 (RA) was one of the top hits, as expected (Fig. S5*B*). Notably, hnRNPLL depletion increased the inclusion of *Irf4* exon 8 in plasma cells, to a degree similar to that observed in naïve B cells (Fig. 6*B*); hnRNPLL has a binding site immediately downstream of this exon in MPC11 cells (Fig. 6*B*), suggesting that this *Irf4* splicing event in plasma cells is directly dependent on hnRNPLL. We

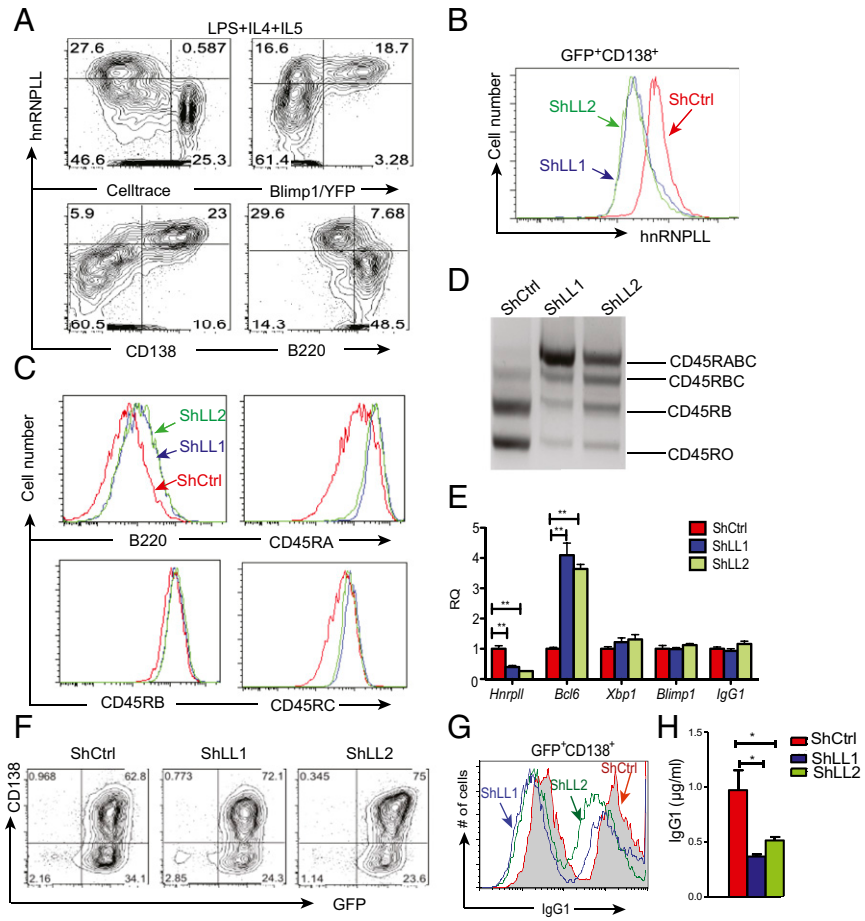

Fig. 5. hnRNPLL is essential for full commitment to the plasma-cell lineage. (*A*) hnRNPLL is highly expressed in plasma cells. CD43$^-$ naïve B cells were isolated from the spleen of Blimp1–YFP reporter mice and stimulated with 10 μg/mL LPS in the presence of IL-4 (10 ng/mL) and IL-5 (10 ng/mL). On day 5 after stimulation, the cells were analyzed for hnRNPLL expression by intracellular staining, together with cell proliferation analysis (measured by Cell Trace Violet dilution), Blimp1–YFP reporter, CD138, and B220 expression. (*B*) Retroviral transduction of sh-RNA against *Hnrpll* efficiently reduced hnRNPLL expression in plasma cells. To deplete *Hnrpll* expression in plasma cells, purified B cells were activated as in *A* and infected twice with retrovirus containing either control (scramble) shRNA (ShCtrl) or two sh-RNAs against *Hnrpll* (ShLL1 and ShLL2) 16 and 40 h after stimulation. Puromycin (1 μg/mL) was added into cell culture 48 h after stimulation. At 5 d after activation, hnRNPLL expression in CD138$^+$GFP$^+$ cells was determined by intracellular staining. (*C* and *D*) hnRNPLL is required for CD45RA exon exclusion during plasma-cell differentiation. (*C*) CD45RA, RB, RC, and B220 expression were compared in GFP$^+$CD138$^+$cells produced 5 d after infection of LPS-stimulated B cells with ShCtrl, ShLL1, or ShLL2 retrovirus. (*D*) CD45 splicing was analyzed by RT-PCR in the GFP$^+$CD138$^+$ cells. PCR products corresponding to each splice isoform of CD45 are indicated. (*E*) hnRNPLL is essential for terminating *Bcl6* expression in plasma cells. CD138$^+$GFP$^+$ cells were purified 6 d after LPS stimulation and analyzed for *Hnrpll*, *Blimp1*, *Xbp1*, *Bcl6*, and *IgG1* expression by real-time RT-PCR. Target gene expression was normalized to that in cells expressing control ShRNA. Error bars show SD of the mean. $^{**}P < 0.01$ by two tailed Student's *t* test. (*F*) hnRNPLL is dispensable for acquisition of CD138 expression during plasma-cell differentiation. As in *B*, 5 d after LPS stimulation, cells infected with shRNA against either *Hnrpll* (ShLL1 and ShLL2) or scramble sequences (ShCtrl) were analyzed for CD138 and GFP expression. Numbers in the graphs show the percentages of the gated populations. (*G* and *H*) hnRNPLL promotes maximal Ig expression in plasma cells. Production of Ig (IgG1) was determined by intracellular staining (*G*) or ELISA (*H*) in CD138$^+$ cells. (*G*) At 6 d after LPS stimulation, GFP$^+$CD138$^+$ cells were gated, and total IgG1 expression was determined by intracellular staining. Data are representative of at least three independent experiments. $^*P < 0.05$ in Student's *t* test.

confirmed binding of hnRNPLL to Irf4 transcripts in activated B cells (Fig. S5*C*). Given the importance of IRF4 in regulating plasma-cell differentiation and function (26, 27), hnRNPLL-regulated alteration in *Irf4* splicing may contribute to certain aspects of plasma-cell differentiation as described above.

We further analyzed gene-expression changes in hnRNPLL-depleted plasma cells. As expected from Fig. 5*E*, *Bcl6* expression was higher in hnRNPLL-depleted cells than in control cells (Fig. 6*C*). Gene Ontology analysis revealed that the most significantly enriched gene set terms in hnRNPLL-depleted plasma cells were genes that are up-regulated from plasmablast to plasma cells ($P < 10^{-6}$; Table S3), further supporting the notion that hnRNPLL mediates terminal differentiation of plasma cells. Diminished expression of genes in this category was further validated by real-time PCR (Fig. 6*D*).

Together, these data indicate that hnRNPLL mediates a large number of alternative splicing events during plasma-cell differentiation, which together promote the transition from plasmablasts into terminally differentiated plasma cells.

hnRNPLL Regulates B-Cell Homeostasis and Plasma-Cell Differentiation in Vivo. To further examine the function of hnRNPLL in B lymphocytes in vivo, we used shRNAs against hnRNPLL to diminish its expression in primary B cells. Briefly, we reconstituted μMT mice, which lack endogenous B cells, with wild-type bone marrow cells transduced with retrovirus containing either sh-hnRNPLL-IRES-GFP (ShLL) or sh-Scramble-IRES-GFP (ShCtrl). Six weeks after reconstitution, GFP$^+$ cells were analyzed. As expected, ∼90% of B cells in the spleen of the chimeric mice expressed GFP and were derived from the donor bone marrow cells (Fig. 7*A*), whereas

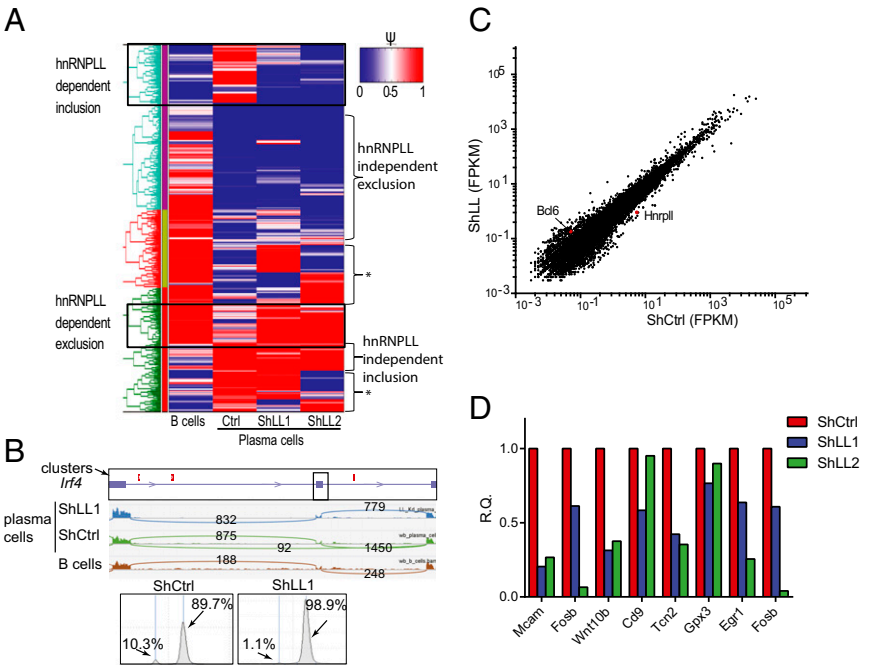

Fig. 6. hnRNPLL mediates global splicing changes during plasma-cell differentiation. (*A*) hnRNPLL is required for a large cohort of alternative splicing changes in plasma cells. Heat map shows the unsupervised hierarchical clustering of plasma-cell–specific splicing changes in B cells, control plasma cells (Sh-scramble), or plasma cells with hnRNPLL depletion (ShLL1 and ShLL2). We first used the MISO algorithm to determine plasma-cell–specific splicing changes of cassette exons ($n = 422$, $\Delta\Psi > 0.2$ or < -0.2 between B cells and control plasma cells), and then calculated Ψ values of these alternative splicing events in hnRNPLL-depleted plasma cells. Two clusters labeled on the left represent hnRNPLL-dependent exon inclusion ($n = 66$) and exon exclusion ($n = 38$), respectively, during plasma-cell differentiation. Only when both shRNAs against hnRNPLL had similar effects were exons defined as hnRNPLL-dependent (highlighted with black boxes). *Cassette exons whose splicing in plasma cells was reverted by only one of two shRNAs against hnRNPLL. (*B*) hnRNPLL mediates a switch of *Irf4* splice isoforms during B-cell to plasma-cell differentiation. (*B*, *Top*) hnRNPLL bound immediately to 3′ of *Irf4* exon 8 based on PAR-CLIP analysis in MPC11 cells. The binding sites are indicated on the top track with red rectangles, the bottom track depicts the Ref-seq annotation, and the alternative exon is boxed. (*B*, *Middle*) IGV genome browser view of RNA-seq data from B cells (brown), plasma cells with ShCtrl (green), or ShRNA to hnRNPLL (blue). Numbers of junctional reads are indicated. Note: In the ShCtrl plasma cells, 92 junctional reads indicated skipping of exon 8 but such events were completely absent in B cells or ShLL plasma cells. (*B*, *Bottom*) Irf4 splicing was analyzed with RT-PCR in plasma cells with either shCtrl or sh hnRNPLL. The result was quantified with the Agilent 2200 TapeStation, and ratios of each isoform are indicated. (*C*) RNA-seq reveals gene expression change between control plasma cells and hnRNPLL-deficient plasma cells. Dot plots show RNA-seq analysis comparing gene expression between plasma cells with ShLL1 and ShCtrl. (*D*) Expression of a group of genes elevated during plasmablasts to plasma-cell transition (Table S3) was further examined by real-time PCR.

there were very few GFP$^+$ cells in other lineages (Fig. 7*A*). Real-time PCR analysis revealed 50% reduction of hnRNPLL expression after shRNA-mediated depletion in B cells. Therefore, in the chimeric mice, only B cells specifically have reduced hnRNPLL expression.

Notably, in the mice given hnRNPLL-depleted bone marrow, both the percentages and the numbers of B cells were significantly reduced compared with those of control mice (~40% and ~50% reduction, respectively) (Fig. 7*A*). The proportion of mature B cells (IgM^{low}IgD^{hi}) in the spleen was also significantly less in the hnRNPLL-depleted mice (Fig. S6). However, analysis of pro- and pre-B cells in the bone marrow did not reveal significant changes between hnRNPLL-depleted and control mice, indicating that hnRNPLL promotes B-cell homeostasis and/or maturation in the periphery.

To further analyze hnRNPLL functions in plasma-cell differentiation and function, we immunized the chimeric mice with 4-hydroxy-3-nitrophenyl conjugated to keyhole limpet hemocyanin (NP-KLH) emulsified with Rubi's adjuvant. Three weeks after immunization, total plasma cells in the bone marrow were shown to express CD138, a cell surface marker of plasma cells (Fig. 7*B*). NP-specific plasma cells were further identified with a NP-specific ELISpot assay (Fig. 7*C*). NP-specific and total plasma cells in the depleted mice were both present in lower numbers than their counterparts in the control mice. In contrast, the frequency of NP-specific antibody-secreting cells in the spleen was comparable between hnRNPLL-depleted and control mice. Thus, hnRNPLL plays a positive role in plasma-cell differentiation and/or homeostasis in vivo, consistent with what we observed in the in vitro differentiation assay.

Discussion

The splicing factor hnRNPLL is highly expressed in terminally differentiated lymphocytes, including plasma cells and effector/memory T cells. In this study, we used PAR-CLIP in the MPC11 plasma cell line to generate a global map of hnRNPLL-binding sites on RNA. Our data reveal that hnRNPLL primarily binds CA repeat elements and, to a lesser extent, other C-, A-, and T-rich motifs, in the introns and 3′ UTRs of mRNAs. We document that, depending on the location of its binding sites on mRNA, hnRNPLL can regulate multiple steps of RNA processing, including exon inclusion, exon exclusion, and RNA stability. We also show that hnRNPLL plays an important role in the terminal differentiation of plasma cells. Although hnRNPLL is dispensable for the initial transition of B cells to the plasma-cell lineage, it has a key role in ensuring that differentiating B cells acquire the full repertoire of plasma-cell properties, including the CD45 isoform switch, termination of Bcl6 expression, exit from the cell cycle, and maximal Ig production. Together, our data indicate that hnRNPLL-mediated RNA processing is essential for the optimal differentiation of B cells into plasma cells and for optimal plasma-cell function.

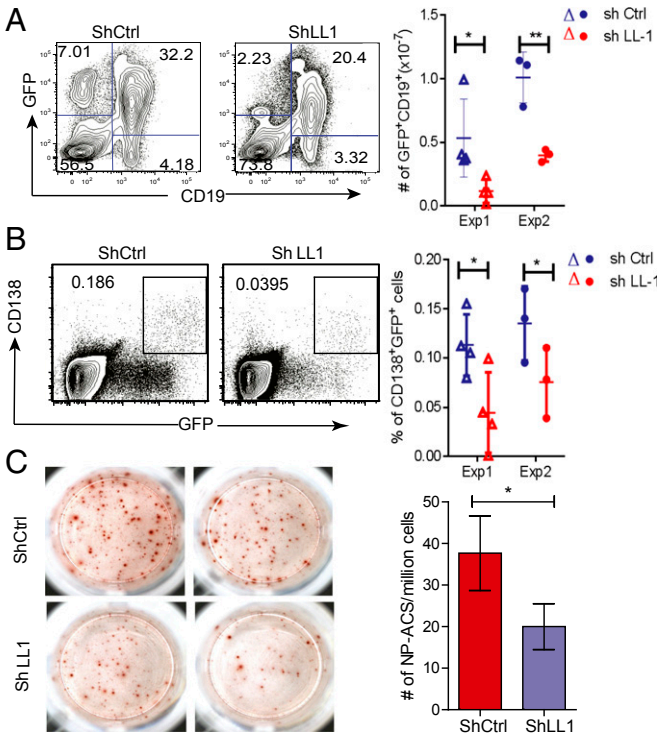

Fig. 7. hnRNPLL promotes B-cell homeostasis and plasma-cell differentiation in vivo. (*A*) hnRNPLL regulates B-cell homeostasis in vivo. μMT mice were reconstituted with WT bone marrow cells transduced with retrovirus containing either sh-LL Puro-IRES-GFP (ShLL1) or sh-scramble Puro-IRES-GFP (ShCtrl). Six weeks after reconstitution, the percentages of B cells (GFP^+ $CD19^+$ cells) in the spleens of chimeric mice were compared, and the total number of GFP^+CD19^+ cells was calculated and summarized in *Right*. Each dot in *Right* represents one individual chimeric mouse from two independent experiments. The vertical line indicates SD of the mean. $^{**}P < 0.01$; $^{*}P < 0.05$ by Student's *t* test. Note the dimmer GFP expression in the mice reconstituted with shLL bone marrow cells, suggesting that cells with the most efficient hnRNPLL depletion have a survival/developmental disadvantage. (*B* and *C*) hnRNPLL deficiency results in reduced plasma cells in the bone marrow after immunization. The chimeric mice were immunized with NP-KLH emulsified with Rubi's (Sigma) adjuvant. Three weeks after immunization, bone marrow cells were analyzed for total plasma cells by CD138 staining (*B*), and the number of NP-specific plasma cells was determined by an Elispot assay (*C*). (*Left*) Representative FACS profile or Elispot pictures. (*Right*) Summary of all of the chimeric mice we analyzed. Error bars depict SD of the mean. $^{**}P < 0.01$; $^{*}P < 0.05$ by Student's *t* test.

There is a growing appreciation of the importance of posttranscriptional regulation in lymphocyte differentiation and gene expression (1). The alternative splicing of CD45RA to CD45RO is one of the hallmarks of memory T-cell differentiation (28). The stability of ICOS mRNA, which is governed by the RBPs Roquin-1 and -2, restrains the differentiation of follicular helper T cells (29–33). The RBPs Zfp36l1 and Zfp36l2 suppress Notch1 mRNA stability, regulating normal thymocyte differentiation and preventing malignant transformation (34). However, most of these studies lack a genome-wide view, an important consideration given the complexity of the RNA-processing network and the need to differentiate between direct and indirect effects caused by the absence of an RBP.

Our study revealed unexpectedly diverse functions of hnRNPLL in posttranscriptional regulation. Specifically, hnRNPLL function appears to be highly dependent on the relative location of its binding site relative to cassette exons in pre-mRNA: When the binding site is 5′ of a cassette exon, hnRNPLL promotes exon inclusion; when it binds 3′ of a cassette exon, it promotes exon exclusion. In addition to binding to introns and exons, hnRNPLL also associates with 3′ UTRs of mRNAs, thereby promoting mRNA stability. Thus, hnRNPLL is a multifaceted RBP.

As observed for many other RBPs (1, 2, 6, 14), the motifs recognized by hnRNPLL are rather degenerate in their sequence. An interesting question is how, given this degeneracy, hnRNPLL achieves specific recognition of its target pre-mRNAs. In our PAR-CLIP analysis, sites of hnRNPLL binding often contained multiple independent T–C conversion events within a single binding cluster, suggesting that hnRNPLL might interact with RNA through multiple protein domains. Indeed, although the (CA)n motif was the most highly enriched in our analysis, other sequence motifs (CTTCC $^{T/}_{C}$, CAT $^{T/}_{A}$ CATT, TTTA $^{T/}_{A}$ A, and an A-rich motif) were also significantly enriched, consistent with the fact that hnRNPLL contains three RRM domains at its N terminus. Further studies will determine whether the three RRM domains of hnRNPLL recognize distinct or similar RNA sequences in their target pre-mRNAs.

Although hnPNPLL appears to be the key hnRNP involved in regulating the exclusion of CD45 exon 4 (encoding CD45RA) in activated T cells (9–11), a near relative, hnRNPL, is responsible for setting basal CD45 exon expression levels (1). hnRNPLL is structurally similar to hnRNPL; moreover, the (CA)n RNA motif we have identified here as recognized by hnRNPLL is similar to the motif identified through SELEX experiments as recognized by hnRNPL (6, 21, 35). Thus, these two related RBPs may have redundant as well as nonoverlapping functions, as confirmed by the overlap in their target genes (e.g., NFAT5) (this work and ref. 6). It will be interesting to examine further the shared vs. independent functions of hnRNPLL and hnRNP L in lymphocytes and other cell types (1). In the case of CD45, hnRNP L and hnRNPLL regulate pre-mRNA splicing by binding in part to the same RNA sequence and in part to distinct RNA sequences in the pre-mRNA (1). Additional studies at single nucleotide resolution in the same cells (i.e., using PAR-CLIP or i-CLIP) will reveal whether recognition of the same as well as distinct sequences is a general property of these related RBPs.

hnRNPL and hnRNPLL both bind 3′ UTRs in addition to introns, thereby increasing mRNA stability (this work and refs. 6, 36, and 37). In a well-studied example, hnRNPL stabilizes VEGF-A mRNA through binding to a CA-rich element in the VEGF-A 3′ UTR (36, 37). Two mechanisms for this phenomenon have been documented: a riboswitch-like mechanism involving mutually exclusive binding of hnRNPL and the GAIT complex (37), and the ability of hnRNPL to block binding of miRNAs to the 3′ UTR (36) (reviewed in ref. 38). It will be interesting to ask whether similar mechanisms are responsible for the ability of hnRNPLL to mediate mRNA stabilization in differentiating B cells.

Depletion of hnRNPLL in B cells and bone marrow cells has diverse physiological effects on plasma-cell differentiation, implying that hnRNPLL controls numerous facets of the B-cell to plasma-cell switch, as also observed in activated T cells (9, 11). Certain early events of plasma-cell differentiation, such as CD138 up-regulation, were unaffected by hnRNPLL depletion; in contrast, later events—including Ig production and *Bcl6* mRNA down-regulation—were clearly influenced by hnRNPLL. Our data show that hnRNPLL directly regulates pre-mRNA splicing of several proteins known to be important for plasma-cell differentiation, including Irf4 and Oct1; further characterization of the functions of these alternatively spliced isoforms in plasma cells will provide a deeper understanding of the role of hnRNPLL and posttranscriptional regulation in the B-cell to plasma-cell switch. In several other cases, however, the mechanism of regulation by hnRNPLL appeared to be indirect. For instance, consistent with our previous finding (12) that hnRNPLL binds IgG1 mRNA in a plasma-cell line, we found that hnRNPLL depletion resulted in decreased Ig production in primary plasma cells (Fig. 5*H*); however, the mRNA level of IgG1 was not significantly

changed after hnRNPLL depletion (Fig. 5*E*), suggesting that hnRNPLL may act directly or indirectly to control the translation rather than the level or stability of IgG1 mRNA.

Chimeric mice reconstituted with hnRNPLL-deficient bone marrow had reduced B-cell compartment in addition to reduced plasma-cell differentiation, indicating additional roles for hnRNPLL in regulating B-cell development and/or homeostasis, similar to its function in T cells (11). Further detailed analysis of B-cell development in hnRNPLL-deficient mice will help elucidate its functions in the various stages of B-cell development.

Previous studies of Bcl6, a transcription factor critical for GC responses (15, 16), have focused primarily on its transcriptional regulation through Blimp1. In contrast, our data point to previously unidentified posttranscriptional mechanisms that govern *Bcl6* expression. Instead of being down-regulated during B- to plasma-cell differentiation, as observed in control cells, *Bcl6* mRNA expression was maintained at high levels in hnRNPLL-depleted cells. Again, however, *Bcl6* mRNA was not directly bound by hnRNPLL, and the splicing patterns of *Bcl6* pre-mRNA were unaltered in hnRNPLL-depleted cells, suggesting that hnRNPLL indirectly facilitates down-regulation of *Bcl6* mRNA during plasma-cell differentiation. Since Irf4 directly suppresses Bcl6 transcription in GC B cells (39), one potential mechanism is that hnRNPLL regulates Bcl6 expression through alternative splicing of *Irf4* transcripts. Posttranscriptional regulation of Bcl6 expression at the protein level may also be involved; an early study comparing resting human B cells versus tonsillar GC B cells showed that *Bcl6* mRNA levels were similar in these two cell types, whereas Bcl6 protein was much more highly expressed in GC B cells (40). Clearly, much remains to be elucidated regarding the posttranscriptional regulation of B-cell to plasma-cell differentiation and the potential role of hnRNPLL in this process.

Materials and Methods

RNA-Seq. Total RNA was isolated with TRIzol (Life Tech). mRNA was selected from ∼10 μg of total RNA with the Ambion MicroPoly(A)Purist Kit or the Ribozero selection kit (Epibio). RNA fragmentation, cDNA conversion, and library preparation were performed by using SOLiD RNA-seq library prep kit (Life Tech). RNA-seq was performed on SOLiD 4 or SOLiD 5500 instruments by using paired-end (50 + 35 bp) sequencing chemistry.

Generation of MPC11 Cell Lines. MPC11 cells were transduced overnight with pLKO.1-shGFP, pLKO.1-sh-hnRNPLL-1, or pLKO.1-sh-hnRNPLL-2 lentivirus and polybrene according to standard protocols in a six-well plate format. After 18 h, medium was removed, and fresh medium with puromycin was added, with selection allowed to occur for 72 h.

PAR-CLIP. PAR-CLIP experiments were conducted as described (6). Briefly, MPC11 cells were pulsed with 4SU (100 μM; Sigma) overnight. After irradiation with UV 365 nm, hnRNPLL/RNA complexes were immunoprecipitated with in-house rabbit anti-hnRNPLL antibody and Protein A Dynal beads (Life Science Tech). After RNase T1 treatment, the immunoprecipitates were resolved on 4–12% LDS gel with Mops buffer (Life Science Tech). RNA on the gel was visualized with SYBR green I staining on the PhosphorImager (GE). RNA was associated with both hnRNPLL isoforms as judged by SYBR green staining, but we focused on RNA bound to the lower isoform. RNA bound to the lower isoform was extracted from the gel, freed from protein by digestion with proteinase K, purified, converted into cDNA, and sequenced by using a SOLiD4 sequencer (50-bp reads).

To derive hnRNPLL-binding clusters, adaptor sequences were first clipped from 3′ ends of sequence reads. Reads that were >20 nt and of quality score >10 were kept for downstream analysis and mapped to the mouse genome (mm9) with Bowtie, allowing maximal two mismatches. Unique mapped reads were kept for downstream analysis.

RNA Extraction, cDNA Synthesis, and Quantitative Real-Time PCR. Total RNA was isolated with the RNeasy plus kit (Qiagen), and cDNA was synthesized by using SuperScript III reverse transcriptase (Life Tech). Quantitative PCR was performed by using the FastStart Universal SYBR Green Master mix (Roche) on a StepOnePlus real-time PCR system (Applied Biosystems). Gene expression was normalized to β-actin. Primers used for qPCR are listed in Table S4.

RNA Immunoprecipitation. B cells were activated with LPS, IL-4, and IL-5 for 4 d and were pulsed with 4SU as in the PAR-CLIP experiments. After irradiation, hnRNPLL/RNA complexes were purified, and RNA was extracted directly from Protein A Dynal beads with TRIZOL reagent. Purified RNA was converted into cDNA, and relative enrichment of target mRNA was determined after normalized to the input and rabbit IgG controls.

Bone Marrow Transplantation. Bone marrow cells were purified from wild-type mice treated with 5-fluorouracil 5 d earlier. The cells were cultured in DMEM with IL-3 (10 ng/mL), IL-6 (20 ng/mL), and Scf (50 ng/mL) and transduced with retrovirus containing the indicated shRNAs in the LMP vector, an murine stem cell virus-based retroviral vector containing an miR30-adapted shRNA backbone, and a phosphoglycerate kinase promoter-driven puroR-IRES-GFP selection cassette (41), at 20 and 40 h after culture. Puromycin (2 μg/mL) was added to the culture on day 3. Cells were harvested on day 5, and 2–5 × 10^6 cells were i.v. injected into μMT mice that had been sublethally irradiated (400 rad) 1 d before cell transfer. Chimeric mice were analyzed 6–8 wk after transplantation.

B-Cell Isolation and in Vitro Differentiation. Naïve B cells were isolated from spleens of C57BL/6 mice. Briefly, splenocytes were treated with red blood cell lysis buffer (155 mM NH_4Cl, 10 mM $NaHCO_3$, and 0.1 mM EDTA), incubated with anti-CD43–PE (BD Biosciences) (1:200) for 30 min on ice, washed with PBS (+1% FBS), and incubated with anti-PE microbeads (Miltenyi Biotec) for 20 min on ice. Naïve B cells were then purified by negative selection using a MACS LS column. Naïve B cells were stimulated with 10 μg/mL LPS (Invivogen), 10 ng/mL IL-4, and 10 ng/mL IL-5 in RPMI 1640 medium (10% FBS, 100 U/mL penicillin, 100 U/mL streptomycin, 50 μM β-mercaptoethanol, and 1% glutamine). Where indicated, naïve B cells were labeled with Cell-Trace Violet (2 nM) before activation.

shRNA-Mediated hnRNPLL Depletion in Primary B Cells. B cells were activated as described above, and on days 2 and 3 after activation, cells were spin-infected with supernatant containing LMP-sh-Scramble, LMP-sh-hnRNPLL-1, or LMP-sh-hnRNPLL-2 retroviruses. Puromycin (2 μg/mL) was added into the culture on day 3, and, when indicated, CD138+ plasma cells were isolated by using anti-CD138–PE and anti-PE MACS beads.

Staining and Flow Cytometry. For cell surface staining, cells were washed with FACS buffer (1% FBS in PBS with 0.1% NaN_3), incubated with the indicated antibodies on ice for 30 min, washed two more times with FACS buffer, and fixed in 1% paraformaldehyde in PBS before being analyzed using BD LSRII or Fortessa machine (BD Biosciences). For intracellular staining, cells were surface stained, fixed/permeabilized with a Cytofix/Cytoperm kit (BD Bioscience), and stained with antibodies against the indicated antigens. Intracellular hnRNPLL staining was carried out by using our in-house hnRNPLL antibody, PE–anti-rabbit IgG (BD Biosciences), and the Foxp3 intracellular staining buffer set (Ebioscience).

ELISpot. To measure NP-specific antibody-secreting cells, Millipore MAHA 96-well filter plates were coated with NP-BSA (50 μg/mL) in PBS at 4 °C overnight. Plates were washed with PBS plus 0.05% Tween 20 twice and blocked with complete DMEM (10% FBS) at 37 °C for 2 h. A total of 1 × 10^7 bone marrow cells were seeded in duplicate in the first well, and two serial dilutions were performed. The plates were then incubated at 37 °C for 5 h. After incubation, plates were washed with PBS and PBS plus Tween 20 each three times, and 0.5 μg/mL biotin anti-mouse IgG was added into each well for overnight incubation at 4 °C. After washing with PBS plus Tween 20, the plates were incubated with Streptavidin–HRP and developed with BD Elispot AREC substrate set according to manufacturer's instruction. The red dots, which were indicative of NP-specific antibody-secreting cells, were counted with computer-assisted image analysis (KS-ELISPOT reader; Zeiss).

Gene Ontology Analysis. To determine the functions of significantly changed transcripts, genes with Log2 (shLL/shCtrl) > 1 or < −1 and fragments per kilobases of transcript per million mapped reads (FPKM) > 0.5 in either control or sh-hnRNPLL samples were analyzed with DAVID, and all genes with FPKM > 0.5 were used as background.

Cluster Analysis of Alternative Splicing Events. The efficiency of splicing of cassette exons was determined by using the MISO algorithm. Splicing events with $\Delta\Psi > 0.2$ or < -0.2 between control plasma cells and B cells were selected. The Ψ values of these splicing events from B cells, control plasma cells, and plasma cells expressing two independent shRNAs against hnRNPLL were clustered by using the K-mean clustering approach.

ACKNOWLEDGMENTS. We thank Prof. Bjoern Peters (head of the La Jolla Institute for Allergy and Immunology Bioinformatics Core) for support, Jeremy Day for next-generation sequencing, Ryan Hastie for technical support, and the LIAI bioinformatics core for constant support and feedback. This work was supported by NIH Grants AI080875, AI040127, and RC4 AI092763 (to A.R.), and HL114093 (to Bjoern Peters and A.R.).

1. Martinez NM, Lynch KW (2013) Control of alternative splicing in immune responses: Many regulators, many predictions, much still to learn. *Immunol Rev* 253(1):216–236.
2. Shukla S, Oberdoerffer S (2012) Co-transcriptional regulation of alternative pre-mRNA splicing. *Biochim Biophys Acta* 1819(7):673–683.
3. Zhang C, et al. (2010) Integrative modeling defines the Nova splicing-regulatory network and its combinatorial controls. *Science* 329(5990):439–443.
4. Licatalosi DD, et al. (2008) HITS-CLIP yields genome-wide insights into brain alternative RNA processing. *Nature* 456(7221):464–469.
5. Yeo GW, et al. (2009) An RNA code for the FOX2 splicing regulator revealed by mapping RNA-protein interactions in stem cells. *Nat Struct Mol Biol* 16(2):130–137.
6. Shankarling G, Cole BS, Mallory MJ, Lynch KW (2014) Transcriptome-wide RNA interaction profiling reveals physical and functional targets of hnRNP L in human T cells. *Mol Cell Biol* 34(1):71–83.
7. Darnell RB (2010) HITS-CLIP: Panoramic views of protein-RNA regulation in living cells. *Wiley Interdiscip Rev RNA* 1(2):266–286.
8. Hafner M, et al. (2010) Transcriptome-wide identification of RNA-binding protein and microRNA target sites by PAR-CLIP. *Cell* 141(1):129–141.
9. Oberdoerffer S, et al. (2008) Regulation of CD45 alternative splicing by heterogeneous ribonucleoprotein, hnRNPLL. *Science* 321(5889):686–691.
10. Topp JD, Jackson J, Melton AA, Lynch KW (2008) A cell-based screen for splicing regulators identifies hnRNP LL as a distinct signal-induced repressor of CD45 variable exon 4. *RNA* 14(10):2038–2049.
11. Wu Z, et al. (2008) Memory T cell RNA rearrangement programmed by heterogeneous nuclear ribonucleoprotein hnRNPLL. *Immunity* 29(6):863–875.
12. Benson MJ, et al. (2012) Heterogeneous nuclear ribonucleoprotein L-like (hnRNPLL) and elongation factor, RNA polymerase II, 2 (ELL2) are regulators of mRNA processing in plasma cells. *Proc Natl Acad Sci USA* 109(40):16252–16257.
13. Kishore S, Luber S, Zavolan M (2010) Deciphering the role of RNA-binding proteins in the post-transcriptional control of gene expression. *Briefings Funct Genomics* 9(5–6): 391–404.
14. Huelga SC, et al. (2012) Integrative genome-wide analysis reveals cooperative regulation of alternative splicing by hnRNP proteins. *Cell Reports* 1(2):167–178.
15. Calame KL, Lin KI, Tunyaplin C (2003) Regulatory mechanisms that determine the development and function of plasma cells. *Annu Rev Immunol* 21:205–230.
16. Nutt SL, Taubenheim N, Hasbold J, Corcoran LM, Hodgkin PD (2011) The genetic network controlling plasma cell differentiation. *Semin Immunol* 23(5):341–349.
17. Ogimoto M, Katagiri T, Hasegawa K, Mizuno K, Yakura H (1993) Induction of CD45 isoform switch in murine B cells by antigen receptor stimulation and by phorbol myristate acetate and ionomycin. *Cell Immunol* 151(1):97–109.
18. Hathcock KS, Hirano H, Murakami S, Hodes RJ (1992) CD45 expression by B cells. Expression of different CD45 isoforms by subpopulations of activated B cells. *J Immunol* 149(7):2286–2294.
19. Sandberg R, Neilson JR, Sarma A, Sharp PA, Burge CB (2008) Proliferating cells express mRNAs with shortened 3′ untranslated regions and fewer microRNA target sites. *Science* 320(5883):1643–1647.
20. Bailey TL, et al. (2009) MEME SUITE: Tools for motif discovery and searching. *Nucleic Acids Res* 37(Web Server issue):W202–W208.
21. Hui J, Stangl K, Lane WS, Bindereif A (2003) HnRNP L stimulates splicing of the eNOS gene by binding to variable-length CA repeats. *Nat Struct Biol* 10(1):33–37.
22. Hoell JI, et al. (2011) RNA targets of wild-type and mutant FET family proteins. *Nat Struct Mol Biol* 18(12):1428–1431.
23. Katz Y, Wang ET, Airoldi EM, Burge CB (2010) Analysis and design of RNA sequencing experiments for identifying isoform regulation. *Nat Methods* 7(12):1009–1015.
24. Hasbold J, Corcoran LM, Tarlinton DM, Tangye SG, Hodgkin PD (2004) Evidence from the generation of immunoglobulin G-secreting cells that stochastic mechanisms regulate lymphocyte differentiation. *Nat Immunol* 5(1):55–63.
25. Shapiro-Shelef M, Calame K (2005) Regulation of plasma-cell development. *Nat Rev Immunol* 5(3):230–242.
26. Teng Y, et al. (2007) IRF4 negatively regulates proliferation of germinal center B cell-derived Burkitt's lymphoma cell lines and induces differentiation toward plasma cells. *Eur J Cell Biol* 86(10):581–589.
27. Klein U, et al. (2006) Transcription factor IRF4 controls plasma cell differentiation and class-switch recombination. *Nat Immunol* 7(7):773–782.
28. Hermiston ML, Xu Z, Weiss A (2003) CD45: A critical regulator of signaling thresholds in immune cells. *Annu Rev Immunol* 21:107–137.
29. Pratama A, et al. (2013) Roquin-2 shares functions with its paralog Roquin-1 in the repression of mRNAs controlling T follicular helper cells and systemic inflammation. *Immunity* 38(4):669–680.
30. Yu D, et al. (2007) Roquin represses autoimmunity by limiting inducible T-cell costimulator messenger RNA. *Nature* 450(7167):299–303.
31. Vinuesa CG, et al. (2005) A RING-type ubiquitin ligase family member required to repress follicular helper T cells and autoimmunity. *Nature* 435(7041):452–458.
32. Glasmacher E, et al. (2010) Roquin binds inducible costimulator mRNA and effectors of mRNA decay to induce microRNA-independent post-transcriptional repression. *Nat Immunol* 11(8):725–733.
33. Vogel KU, et al. (2013) Roquin paralogs 1 and 2 redundantly repress the Icos and Ox40 costimulator mRNAs and control follicular helper T cell differentiation. *Immunity* 38(4):655–668.
34. Hodson DJ, et al. (2010) Deletion of the RNA-binding proteins ZFP36L1 and ZFP36L2 leads to perturbed thymic development and T lymphoblastic leukemia. *Nat Immunol* 11(8):717–724.
35. Hui J, et al. (2005) Intronic CA-repeat and CA-rich elements: A new class of regulators of mammalian alternative splicing. *EMBO J* 24(11):1988–1998.
36. Jafarifar F, Yao P, Eswarappa SM, Fox PL (2011) Repression of VEGFA by CA-rich element-binding microRNAs is modulated by hnRNP L. *EMBO J* 30(7):1324–1334.
37. Ray PS, et al. (2009) A stress-responsive RNA switch regulates VEGFA expression. *Nature* 457(7231):915–919.
38. Jia J, Yao P, Arif A, Fox PL (2013) Regulation and dysregulation of 3′UTR-mediated translational control. *Curr Opin Genet Dev* 23(1):29–34.
39. Saito M, et al. (2007) A signaling pathway mediating downregulation of BCL6 in germinal center B cells is blocked by BCL6 gene alterations in B cell lymphoma. *Cancer Cell* 12(3):280–292.
40. Allman D, et al. (1996) BCL-6 expression during B-cell activation. *Blood* 87(12): 5257–5268.
41. Dickins RA, et al. (2005) Probing tumor phenotypes using stable and regulated synthetic microRNA precursors. *Nat Genet* 37(11):1289–1295.
42. Huang W, Sherman BT, Lempicki RA (2009) Systematic and integrative analysis of large gene lists using DAVID bioinformatics resources. *Nat Protoc* 4(1):44–57.